arXiv:0802.3026v1 [astro-ph] 21 Feb 2008

To investigate the nature M1–78 further, we present a detailed spectroscopic study of M1–78 in the optical and near-infrared. We obtained long-slit, intermediate-resolution, optical spectroscopy with the ISIS spectrograph mounted on the William Herschel Telescope (WHT) at Roque de los Muchachos Observatory (La Palma, Spain). As a complement, we obtained long-slit, intermediate-resolution, near-infrared spectra using LIRIS, the near-infrared imager/spectrographer also installed at the WHT. M1–78 is a high-density nebula with substantial physical differences between its two main morphological zones: a bright arc to the SW and a blob of emission in the NE. Specifically, the blob in the NE has a higher electron temperature (13400 K) and visual extinction (about 9 mag) than the SW arc. The most important result, however, is the confirmation of a nitrogen enrichment in M1–78. This enrichment is stronger at the location of the NE blob and is correlated with a defficiency in the O abundance and a (dubious) He enrichment. Such an abundance pattern is typical of ejecta nebulae around evolved massive stars such as Wolf–Rayet and Luminous Blue Variable stars. The spatial variations in the physical conditions and chemical abundances and the presence of more than one possible ionizing source indicates, however, that M1–78 is better described as a combination of a compact H II region + ejecta. This is confirmed by the He I 2.112 μm/Brγ line ratio, which indicates a hot ($T_{eff} \gtrsim 40000$ K) O star in the SW arc. Finally, we detect H_2 emission that extends over a large ($\sim 30''$) area around the ionized nebula. Analysis of the near-infrared H_2 lines indicates that the excitation mechanism is UV fluorescence.

Key words. Infrared: ISM – ISM: individual objects: M1-78 – ISM: HII regions – ISM: abundances – Stars: early type – Stars: Wolf-Rayet

Astronomy & Astrophysics manuscript no. 9039
(DOI: will be inserted by hand later)

February 21, 2008

M1–78: a nitrogen-rich Galactic compact H II region beyond the Perseus arm

N. L. Martín-Hernández[1], C. Esteban[1], A. Mesa-Delgado[1], A. Bik[2], and E. Puga[3]

[1] Instituto de Astronomía de Canarias, Vía Láctea s/n, 38205 La Laguna, Spain
[2] European Southern Observatory, Karl-Schwarzschild Strasse 2, 85748 Garching-bei-München, Germany
[3] Instituut voor Sterrenkunde, Katholieke Universiteit Leuven, Celestijnenlaan 200B, 3001 Leuven, Belgium

Received; accepted

Abstract. There is considerable controversy surrounding the nature of M1–78, a compact nebula located beyond the Perseus arm. It was first classified as a planetary nebula and is nowadays generally considered to be a compact H II region.

1. Introduction

M1–78 (another designation is IRAS 21190+5140) was first observed by Minkowski (1946) in a survey of emission-line objects and is nowadays generally classified as an H II region. Nevertheless, it is still listed in the *Simbad Astronomical Database*[1] as a "possible planetary nebula" (PN), which reflects the controvery that has existed around the nature of this source. The survey of Latter et al. (1995) catalogues this object as a middle-butterfly PN, where a butterfly or bipolar nebula is a PN that is bi-lobed and has an equatorial waist. Phillips (2004) places this source at a distance of 1.6 kpc using the correlation between 5 GHz brightness temperatures and intrinsic radio luminosities established for PNe and based on stellar evolutionary models. However, the distance determined by Puche et al. (1988) based on the H I absorption spectrum is in between 5 and 8 kpc, beyond both the Local arm and the Perseus arm. This is in agreement with the kinematic distance of 8.9 kpc obtained from its radial velocity (e.g. Peeters et al., 2002). Such a distance implies a high luminosity of about 2×10^5 L/L$_\odot$ (see again Peeters et al., 2002), which makes the classification of M1–78 as a PN untenable, as pointed out already by Zijlstra et al. (1990) and Gussie (1995). A classification as an ultracompact H II region is favored instead by these authors. Gussie (1995) even favors a rather unique classification for this region, that of an ultracompact H II region with a post-main sequence central star, probably a Wolf-Rayet (WR) star, based on the high expansion velocity of the nebula (around 25 km s^{-1}) and a possible overabundance of nitrogen (see also Perinotto, 1991).

Several near-infrared (NIR) spectra of M1–78 have been obtained showing emission of atomic hydrogen and helium and molecular hydrogen (e.g. Hora et al., 1999; Lumsden et al., 2001a,b). This source has also been imaged in the NIR (e.g. Latter et al., 1995), mid-infrared (e.g. Peeters, 2002) and radio (e.g. Zijlstra et al., 1990), showing a similar morphology at all wavelengths, i.e. an overall structure emcompassing a prominent arc of which the tail at both sides converges towards a blob of emission to the NE (see Fig. 1). The ISO spectrum of this object is rather unique and shows silicate in emission at about 10 and 20 μm (Peeters et al., 2002). In addition, it shows strong emission features generally attibuted to emission by polyclyclic aromatic hydrocarbon (PAH) molecules, typical of H II regions (cf. Peeters et al., 2002).

We obtained long-slit, intermediate-resolution, optical spectroscopy with the ISIS spectrograph mounted on the 4.2 m William Herschel Telescope (WHT) at Roque de los Muchachos Observatory (La Palma, Spain). As a complement, we obtained long-slit, intermediate-resolution, NIR spectra of M1–78 using LIRIS, the NIR imager/spectrographer also mounted on the WHT. The aim of this study is to investigate the controversial nature of M1–78.

This paper is structured as follows. Section 2 describes the observations and data reduction. Section 3 and Sect. 4 present the results of the optical and NIR data, respectively. Section 5 discusses the nature of M1–78 and Sect. 6 summarizes the main conclusions.

2. Observations and data reduction

2.1. Optical observations

Intermediate-resolution spectroscopy was obtained on 2007 July 18 with the ISIS spectrograph mounted on the 4.2 m William Herschel Telescope (WHT) at Roque de los Muchachos Observatory (La Palma, Spain). Two different CCDs were used at the blue and red arms of the spectrograph: an EEV CCD with a configuration 4100 × 2048 pixels with a pixel size of 13.5 μm in the blue arm and a REDPLUS CCD with 4096 × 2048 pixels with a pixel size of 15 μm in the red

---

Send offprint requests to: N.L. Martín-Hernández, leticia@iac.es

[1] http://simbad.u-strasbg.fr/simbad/

arm. The dichroic used to separate the blue and red beams was set at 5300 Å. The slit was 3′.7 long and 1″.03 wide. Two gratings were used, the R1200B in the blue arm and the R316R in the red arm. These gratings give reciprocal dispersions of 17 and 62 Å mm^{-1}, and effective spectral resolutions of 0.86 and 3.56 Å for the blue and red arms, respectively. The blue spectra cover from $\lambda\lambda$4225 to 5075 Å and the red ones from $\lambda\lambda$5335 to 8090 Å. The spatial scale is 0″.20 pixel^{-1} and 0″.22 pixel^{-1} in the blue and red arms, respectively. The average seeing during the observations was ∼0″.8.

We observed a single slit position centered on the brightest nebular spot (see Fig. 1) and with a position angle P.A.=50°. We took three consecutive 600 s exposures in both arms in order to get a reasonably good spectrum of this faint object. The data were wavelength calibrated with a CuNe+CuAr lamp. The correction for atmospheric extinction was performed using the average curve for continuous atmospheric extinction at Roque de los Muchachos Observatory. The absolute flux calibration was achieved by observations of the standard stars BD+33 2642, BD+28 4211 and BD+25 4655. All the CCD frames were reduced using the standard IRAF[2] TWODSPEC reduction package to perform bias correction, flat-fielding, cosmic-ray rejection, wavelength and flux calibration, and sky subtraction.

2.2. NIR observations

NIR spectra in the 2.0–2.4 μm wavelength range (K-band) were obtained on the night of 2006 September 9 at the 4.2 m WHT using LIRIS, a long-slit, intermediate-resolution, infrared spectrograph (Acosta Pulido et al., 2003; Manchado et al., 2004). The spectral region blueward of about 1.98 μm is affected by substantially degraded atmospheric transmission. LIRIS is equipped with a Rockwell Hawaii 1024 × 1024 HgCdTe array detector. The spatial scale is 0″.25 pixel^{-1}, and the slit width used during the observations was 0″.75, allowing a spectral resolution $R = \lambda/\Delta\lambda \sim 1000$. The slit was orientated along P.A.= 50° (slit #1, which corresponds to the single-slit observed in the optical) and 140° (slit #2) centered on the brightest nebular spot (see Fig. 1). Weather conditions were relatively good, although with sparse cirrus. The seeing during our observations varied between 0″.8 and 1″.3 measured from the FWHM of the standard star spectra.

Observations were performed following an ABBA telescope-nodding pattern, placing the source in two positions along the slit, separated by 45″. Individual frames were taken with integration times of 300 s and total on-source integration times of 30 minutes for slit #1 and 20 minutes for slit #2. In order to obtain the telluric correction and the flux calibration, the nearby HIP 106393 A0 V star was observed with the same configuration. The data were reduced following standard procedures for NIR spectroscopy, using IRAF and LIRISDR, the LIRIS Data Reduction package. After the flat-field correction, consecutive pairs of AB two-dimensional spectra were subtracted to remove the sky background. The resulting frames were then co-added to provide the final spectrum. Sky lines present in the science data were used to determine the wavelength calibration. The final uncertainty in the wavelength calibration is roughly 1Å. The resulting wavelength-calibrated spectra were divided by a composite spectrum to remove the telluric contamination. This composite spectrum was generated from the observed spectra of HIP 106393, divided by a Vega model convolved with the actual spectral resolution (∼ 23Å) using the routine *xtellcor_general* within the Spextool package[3], an IDL-based spectral reduction tool written by Mike Cushing and Bill Vacca. This routine is also used for the flux calibration, which is done by normalizing with the B and V magnitudes of the standard star provided by the *Simbad Astronomical Database* (B=5.734 and V=5.766). We estimate an uncertainty in the flux calibration around 40% based on the comparison of the various spectra obtained for the standard star.

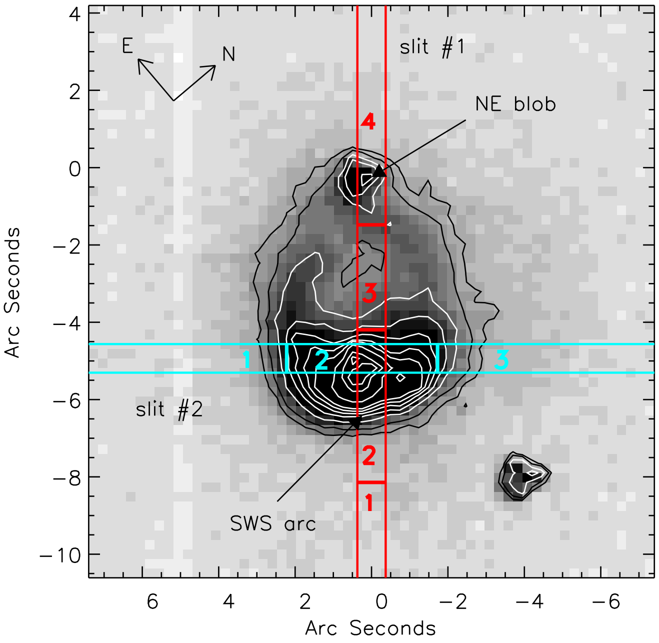

Fig. 1. NIR broad-band (Ks filter) acquisition image of M1–78. The positions of the NIR slits (in red slit #1 with a P.A. of 50°, and in cyan slit #2 with a P.A. of 140°) are marked. The (0″,0″) position corresponds to R.A.=21^{h}20^{m}44.91^s and Dec.=+51^{d}53^{m}27.3^s (J2000.0). The H_2 regions analysed in Sect. 4.7 are indicated. At a distance of 8.9 kpc, 1″ corresponds to 0.043 pc.

3. Results from optical observations

3.1. Features of the optical spectra

The two-dimensional optical spectrum shows two peaks in the surface brightness distribution of the emission lines along the

---

[2] IRAF is distributed by the National Optical Astronomy Observatory, which is operated by the Association of Universities for the Research in Astronomy, Inc., under cooperative agreement with the National Science Foundation (http://iraf.noao.edu/).

[3] http://irtfweb.ifa.hawaii.edu/∼spex/

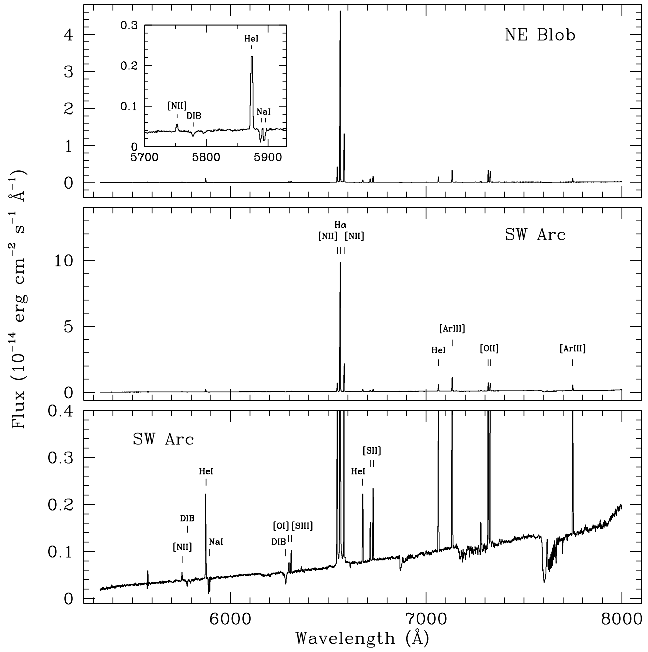

Fig. 2. Red range of the optical spectra extracted from a slit position coincident with slit #1 of the NIR observations (see Fig. 1). The upper panel corresponds to the emission of the NE blob; the inset show an enlargment of the spectral area around the [N ii] 5755 Å and He i 5876 Å lines. The middle and the lower panels show the red spectrum of the SW arc at different line-flux levels. The fluxes are not corrected for reddening. The identification of most emission lines and absorption features are indicated. The broad absorption features longward 6800 Å are due to the atmosphere.

spatial direction. These peaks coincide with the two main morphological zones of the nebula: the brightest arc to the SW and the blob of emission to the NE. In addition, each peak contains a featureless, very weak and unresolved stellar continuum (note that the nebular contribution to the continuum in the optical is generally very small). Only the continuum associated with the SW arc – brightest one – is detected in the spectrum of the blue arm. We extracted two one-dimensional spectra isolating the emission from each peak, the spatial extension of each zone being 4″.4. The spectra of the red range of both zones are shown in Fig. 2. A detailed inspection of the emission line profiles along the slit does not show any evidence of stellar features or broad components in the recombination-line profiles due to the contribution of photospheric emission of massive stars.

Line intensities were measured integrating all the flux in the line between two given limits and over a local continuum estimated by eye and using the SPLOT routine of the IRAF package. The line intensities of the blue arm spectra were normalized to that of Hβ, while those of the red arm were normalized to Hα. The reddening coefficient, c(Hβ), was determined by fitting the observed I(Hγ)/I(Hβ) ratio of the spectra of the blue arm to the theoretical line ratio obtained from the calculations of Storey & Hummer (1995), assuming case B, and electron temperature and density of 10^4 K and $n_e = 10^3$ cm^{-3}. We considered the reddening law of Whitford (1958). Once the reddening was derived, the emission line ratios of the red spectra were re-scaled to the I(Hβ). The spectrum of the NE blob shows a somewhat larger reddening coefficient, indicating a larger amount of internal dust in this zone of M1–78 that produces an extinction A_V of about 9 mag. Our determinations of c(Hβ) are consistent with the value of 4.1 found by Aller & Keyes (1987). Lumsden et al. (2001b) derived a similar extinction in the NIR of $A_V \sim 6.5$ mag (assuming $R_V = 3$; Mathis, 1990) estimated by comparing the higher Brackett series lines with Brγ and assuming an exponential extinction law $A_\lambda \propto \lambda^{-1.85}$.

In Table 1 we include, for the two extracted areas, the observed and laboratory wavelength of the identified lines, their reddening-corrected intensity ratios with respect to Hβ, the corresponding values of the reddening function, $f(\lambda)$, for each emision line, the reddening coefficient c(Hβ), the observed Hβ line flux and the physical conditions of the gas – electron density and temperature – determined from different emission-line ratios. We performed a single Gaussian fit of the profiles of the brightest lines of the blue range of the spectra (Hβ and [O iii] 4959 and 5007 Å) for determining the radial velocity of the nebula with respect to the local standard of rest (LSR), finding a value of −74±1 and −70±2 km s^{-1} for the SW arc and the NE blob, respectively. These values are in good agreement with the $v_{\rm LSR} = -76\pm2$ km s^{-1} found by Gussie & Taylor (1989) also from optical spectroscopic observations and with measurements of hydrogen radio recombination lines obtained by Terzian et al. (1974) and Churchwell et al. (1976).

The red spectrum of the NE blob shows several uncommon permitted faint emission lines that were identified as O i 7254 Å (a blend of three unresolved lines at 7254.14, 7254.45 and 7254.53 Å), O i 7002 Å (a blend of 7001.92 and 7002.23 Å) and O i 6046 Å (a blend of 6046.23, 6046.44 and 6046.49 Å), belonging to multiplets no. 20, 21 and 22, respectively; N i 7442 and 7468 Å of multiplet no. 3; and Si ii 6347 and 6371 Å of multiplet no. 3. As demonstrated by Grandi (1975, 1976), all these lines come from upper levels of their respective ions that can be excited from the ground state by the absorption of stellar photons longward of 912 Å. Also, it is important to note that all these lines are precisely the brightest permitted ones of O i, N i and Si ii in the Orion Nebula (see Esteban et al., 2004), although their line ratios with respect to Hβ are larger in M1–78 than in the Orion Nebula. These permitted lines are produced in the vicinity of the transition zone of the nebula, where the fraction of neutral material becomes important and are rather uncommnon in PN (e.g. Liu et al., 2004), where they should be presumably produced in dense clumps or globules of neutral material embedded inside the ionized gas (Grandi, 1976). Other interesting lines in the spectra of M1–78 are those of [Fe ii] 7155 Å (multiplet 14F, only detected in the NE blob) and [Ni ii] 7378 Å (multiplet 2F, detected in both spectra). Both are also the brightest forbidden lines of those ions in the Orion Nebula in the spectral range covered by our red arm spectrum (Esteban et al., 2004). Lucy (1995) and Bautista et al. (1996) demonstrate that, in the Orion Nebula, these lines are produced by the absorption of stellar non-ionizing UV photons. Interestingly, these lines, especially those of [Ni ii], are very strong in the circumstellar ejecta around the Luminous Blue

Table 1. Dereddened line intensity ratios with respect to $I(\mathrm{H}\beta)$ =100, reddening coeeficient, observed Hβ flux and physical conditions obtained from the optical spectra.

			SW arc		NE blob	
λ_0(Å)	Identification	$f(\lambda)$	λ_{obs}(Å)	$I(\lambda)/I(\mathrm{H}\beta)$	λ_{obs}(Å)	$I(\lambda)/I(\mathrm{H}\beta)$
4340.47	Hγ	0.135	4339.00	47.0 ± 2.5	4339.04	47.0 ± 3.9
4471.48	He i	0.10	4470.09	4.0 ± 0.8	...	...
4861.33	Hβ	0.00	4859.73	100 ± 2	4859.77	100 ± 2
4921.93	He i	-0.01	4920.42	9.2:	...	...
4958.91	[O iii]	-0.02	4957.30	134.6 ± 3.8	4957.38	93.6 ± 2.7
5006.84	[O iii]	-0.03	5005.17	372.1 ± 8.3	5005.26	258.3 ± 5.8
5015.68	He i	-0.03	5013.99	2.1 ± 0.4	5014.15	2.0 ± 0.4
5517.71	[Cl iii]	-0.17	...	...	5516.19	0.8 ± 0.2
5537.88	[Cl iii]	-0.18	...	...	5536.28	1.0 ± 0.2
5754.64	[N ii]	-0.21	5752.77	1.3 ± 0.2	5752.69	2.5 ± 0.1
5875.67	He i	-0.23	5873.75	11.4 ± 0.4	5873.72	19.8 ± 0.6
6046.44	O i	-0.26	...	...	6044.87	2.5:
6300.30	[O i]	-0.30	6298.55	0.9 ± 0.1	6298.50	2.4 ± 0.1
6312.10	[S iii]	-0.30	6310.38	1.8 ± 0.1	6310.27	2.4 ± 0.1
6363.78	[O i]	-0.31	6362.32	0.2:	6361.96	0.7 ± 0.1
6571.36	Si ii	-0.31	...	...	6370.07	2.9 0.7 ± 0.4
6548.03	[N ii]	-0.34	6546.10	18.5 ± 0.5	6546.02	26.4 ± 0.8
6562.82	Hα	-0.34	6560.85	286.0 ± 5.9	6560.74	286.0 ± 5.9
6583.41	[N ii]	-0.34	6581.41	59.4 ± 1.3	6581.32	59.4 ± 1.3
6678.15	He i	-0.35	6676.08	3.8 ± 0.1	6676.00	3.8 ± 0.1
6716.47	[S ii]	-0.36	6714.33	2.1 ± 0.1	6714.05	2.1 ± 0.1
6730.85	[S ii]	-0.36	6728.76	3.8 ± 0.1	6728.46	3.8 ± 0.1
7001.92	O i	-0.39	...	...	6999.58	0.2:
7065.28	He i	-0.40	7062.74	8.8 ± 0.3	7062.70	8.8 ± 0.3
7135.78	[Ar iii]	-0.41	7133.23	17.4 ± 0.5	7133.11	17.4 ± 0.5
7155.14	[Fe ii]	-0.41	...	...	7152.25	0.1:
7254.35[a]	O i	-0.42	...	...	7251.66	2.3 ± 0.8
7281.35	He i	-0.43	7279.25	1.0 ± 0.2	7278.96	0.43 ± 0.04
7318.39	[O ii]	-0.43	7317.43	9.8 ± 0.4	7317.18	8.7 ± 0.3
7329.66	[O ii]	-0.43	7327.83	9.1 ± 0.3	7327.59	7.5 ± 0.2
7377.83	[Ni ii]	-0.44	7375.68	0.2:	7374.98	0.20 ± 0.02
7442.30	N i	-0.44	...	...	7438.75	0.09 ± 0.02
7468.31	N i	-0.45	...	...	7465.74	0.15 ± 0.03
7751.10	[Ar iii]	-0.48	7748.92	4.5 ± 0.1	7748.79	1.56 ± 0.06
$c(\mathrm{H}\beta)$			3.09 ± 0.02		4.10 ± 0.04	
$F(\mathrm{H}\beta)$[b]			160 ± 3		73 ± 2	
n_{e}([S ii])[c]			6700 ± 1000		6400 ± 1200	
n_{e}([Cl iii])[c]			...		5400^{+8800}_{-900}	
T_{e}([N ii])[d]			10900 ± 600		13400 ± 400	

(a) Blend of O i lines at 7254.14, 7254.45 and 7254.53 Å. (b) Observed (uncorrected) flux in units of $10^{-}16$ erg cm^{-2} s^{-1}. (c) In cm^{-3}. (d) In K.

Variable (LBV) star P Cygni (Johnson et al., 1992) and another two nebulosities associated with LBV stars in the LMC (Stahl & Wolf, 1986). Stellar fluorescence also seems to be the most likely excitation mechanism of [Ni ii] lines in those nebulae (Lucy, 1995).

As it can be seen in Fig. 2, both one-dimensional spectra show clear absorption features. Although the most conspicuous ones are atmospheric bands, the narrower features are of interstellar origin. We identified the Na i doublet at 5890 and 5896 Å, the K i doublet at 7665 and 7699 Å, and several diffuse interstellar bands (DIBs) at 5780, 5797, 6177, 6284, 6379 and 6614 Å. We determined the LSR velocities of the centroids of the single Gaussian fits of the interstellar absorption features comparing the observed and rest frame wavelengths (for the DIBs, we used the precise wavelengths of Galazutdinov et al., 2000). The v_{LSR} values we found are in the range −68 to −32 km s^{-1}, consistent with the velocities of the H i absorption features observed by Puche et al. (1988) and identified as caused by neutral gas in and beyond the Perseus spiral arm. The relatively high negative radial velocity of the nebula and the presence of these interstellar absorption systems in the line of sight of the

Table 2. Ionic and total abundances derived from optical lines.

	SW arc	NE blob
12+log(O^{+}/H^{+})	7.81 ± 0.17	7.31 ± 0.10
12+log(O^{++}/H^{+})	8.00 ± 0.09	7.59 ± 0.05
12+log(O/H)	8.24 ± 0.10	7.77 ± 0.06
12+log(N^{+}/H^{+})	7.00 ± 0.07	6.93 ± 0.04
log(N/O)	−0.81 ± 0.21	−0.38 ± 0.12
12+log(S^{+}/H^{+})	5.43 ± 0.10	5.52 ± 0.07
12+log(S^{++}/H^{+})	6.47 ± 0.12	6.27 ± 0.06
12+log(S/H)	6.53 ± 0.12	6.39 ± 0.06
log(S/O)	−1.69 ± 0.14	−1.38 ± 0.09
12+log(Ar^{++}/H^{+})	6.11 ± 0.07	5.70 ± 0.05
12+log(Cl^{++}/H^{+})	...	4.78 ± 0.13
He^{+}/H^{+} (4471)	0.078 ± 0.019	...
He^{+}/H^{+} (5876)	0.077 ± 0.005	0.119 ± 0.006
He^{+}/H^{+} (6678)	0.097 ± 0.006	0.083 ± 0.004
He^{+}/H^{+} (7065)	0.175 ± 0.019	0.079 ± 0.010
<He^{+}/H^{+}>$^{(a)}$	0.084 ± 0.009	0.101 ± 0.018
He/H	0.091 ± 0.009	0.123 ± 0.018

$^{(a)}$ Mean value excluding He^{+}/H^{+} (7065 Å).

object clearly indicate that M1–78 is a rather distant Galactic object.

3.2. Physical conditions and chemical abundances

The physical conditions of the nebula, electron density and temperature were derived with the IRAF task TEMDEN of the package NEBULAR, based in the FIVEL program developed by De Robertis et al. (1987) and improved by Shaw & Dufour (1995). The electron density, n_e, was calculated from the [S ii] 6717/6731 line ratio in the two one-dimensional spectra as well as the [Cl iii] 5518/5538 line ratio in the spectrum of the NE blob. The densities found are very high and similar in both zones, 6700 and 6400 cm^{-3} for the arc and the blob, respectively (see Table 1), and are roughly consistent but slightly higher than previous determinations based on optical (∼ 2500 cm^{-3}, Aller & Keyes, 1987) or far-infrared spectroscopy (∼ 3000 cm^{-3}, Martín-Hernández et al., 2002). These large values of n_e are common in compact H ii regions and are also on the order of those observed in the Orion Nebula (e.g. Esteban et al., 1998).

Although the excitation degree of M1–78 is rather high and the optical nebular [O iii] lines are strong, the auroral [O iii] 4363 Å line cannot be detected due to the large dust extinction. Fortunately, the temperature sensitive [N ii] 5755 Å line was measured with a rather good signal-to-noise ratio in both zones and therefore we could obtain a direct determination of the electron temperature, T_e, in M1–78. The values of T_e are included in Table 1. It can be seen that the temperature is substantially different in the two zones; the NE blob shows T_e = 13400 K, which is atypically high for a Galactic H ii region. A previous determination of the temperature was obtained by Aller & Keyes (1987), who found T_e = 11300 K – probably determined from the [O ii] line ratio – in agreement with the values we obtain for the SW arc. Since the intensity of the [N ii] 5755 Å line could suffer from some contribution due to recombination, we estimated this contribution using the expression obtained by Liu et al. (2000) and find that it is negligible, approximately 0.4% and 0.2% for the arc and the blob zones, respectively.

Ionic abundances of N^{+}, O^{+}, O^{++}, S^{+}, S^{++}, Ar^{++} and Cl^{++} were derived from collisionally excited lines by making use of the IRAF task IONIC of the package NEBULAR. In the absence of temperature determinations for further ions, we considered a one-zone scheme, assuming that the temperature obtained from the [N ii] line ratio is valid for the rest of the ions in the nebula. We measured several He i lines in our spectra. These lines arise mainly from recombination but they can be affected by collisonal excitation and self-absorption effects. We derived the He^{+}/H^{+} ratio using the effective recombination coefficients given by Pequignot et al. (1991) and applying the collisional corrections proposed by Kingdon & Ferland (1995). The final adopted value for the He^{+} abundance is the mean of the values obtained for the brightest individual He i lines but excluding He i 7065 Å, which suffers from the largest collisional effects. All the ionic abundances are included in Table 2.

Since we do not detect He ii lines, we expect that the contribution of O^{3+} should be negligible, and the total O abundance was therefore determined by just adding the ionic abundances of O^{+} and O^{++}. As can be seen in Table 2, the O/H ratio obtained for the two zones of the nebula is very different, the SW arc shows a value consistent with that expected by the radial Galactic abundance gradient of e.g. Deharveng et al. (2000) for a galactocentric distance of 12.7 kpc. However, the spectrum of the NE blob shows an O/H ratio a factor of 3 lower than that of the arc. Aller & Keyes (1987) also find a relatively low O abundance for the object (12+log(O/H) = 8.07).

The observed N^{+}/O^{+} ratio – that is usually assumed to be equal to the N/O ratio due to the similar ionization potential of both ions – is high in both areas of the nebula, especially in the blob, where log(N^{+}/O^{+}) = −0.38. The expected value of log(N/O) at the distance of the nebula should be about −1.2 (e.g. Shaver et al., 1983), indicating that the nebula is nitrogen-rich by factors as large as 6 in the NE blob. The presence of nitrogen enrichment in the object has been indicated by several authors, such as Zijlstra et al. (1990) and Perinotto (1991).

We also estimated the total abundances of He and S by making use of an appropriate ionization correction factor, *icf*, scheme for each element. These factors account for the contribution of the abundances of unseen ionization stages of each chemical element. In the case of He, we used the *icf* proposed by Peimbert et al. (1992), based on the similarity of the ionization potentials of He^{0} and S^{+}. This *icf* seems to work well for relatively high excitation objects like M1–78, where only a small fraction of He^{0} is expected. In the case of S, we have to consider some contribution for unseen S^{3+} and we assume the correction proposed by Stasinska (1978). The equations of both *icf*s can be found in García-Rojas et al. (2004). As shown in Table 2, the S/H ratios of the two one-dimensional spectra differ by only 40% (0.14 dex) and can be considered rather similar within the errors. The fact that the total abundance of S does not show the behavior of the O/H ratio seems to support that the difference of O abundance in both zones of the nebula could be real and not an artefact produced by, for example, a localized abnormally high T_e. On the other hand, the He/H ratio seems to be somewhat higher (34%) in the NE blob than in the SW arc. However, this difference is produced entirely by the different He^+/H^+ ratio obtained from the He I 5876 Å line in both spectra and is not correlated with similar differences in the abundance obtained from the other He I lines. Therefore, we consider the different He/H to be dubious.

4. Results from NIR observations

4.1. Features of the NIR spectra

Figure 3 shows the integrated nebular spectra of M1–78 along slits #1 and #2. The most obvious features in the spectra are the Brγ line, a large set of H I Pfund lines, several He I emission lines and a relatively large number of molecular hydrogen transitions. Three forbidden lines of [Fe III] are also evident. Table 3 lists the observed lines, their identifications and fluxes. The quoted uncertainties are those coming from the line fitting procedure. Peak positions, equivalent widths and fluxes of the lines were measure by fitting a Gaussian profile. A line was defined as being detected if its peak intensity exceeds the rms noise level of the local continuum by at least a factor of 3.

The validity of our flux calibration can be checked by comparing the value we obtain for the Brγ line flux with previous spectroscopic observations. Hora et al. (1999) measured a flux of 1110×10^{-18} W m^{-2} with a $1'' \times 6''$ slit orientated north–south and centered on the brightest infrared portion of the source. Similarly, Lumsden et al. (2001b) measured 1430×10^{-18} W m^{-2} integrating over a region $1\farcs2 \times 12\farcs6$. These values are comparable to the flux we observe for Brγ and list in Table 3.

4.2. The spatial variation of NIR emission lines

Figure 4 illustrates the spatial variation of Brγ, the strongest He I lines (at 2.058 and 2.112 μm) and the H_2 1-0 S(1) transition at 2.121 μm. The ionized gas traced by Brγ distributes along $\sim 7\farcs5$ of slit #1 and $\sim 4''$ of slit #2. Similarly to the optical observations, the two-dimensional NIR spectrum along slit #1 shows two peaks in the surface brightness distribution of the emission lines that correspond to the NE blob and the SW arc. Also within these peaks, we detect a featureless and weak continuum, specifically at the ($0''$,$0''$) and ($0''$,$-5''$) locations. Spectra extracted from $0\farcs75 \times 0\farcs75$ regions around these continua are shown in Fig. 3.

We investigated the nature of the continua detected in the K-band. NIR continuum can be produced not only by a stellar photosphere but also by: (1) the free–free and free–bound emission from ionized gas, (2) hot dust and (3) scattered light, i.e. radiation escaping through optically thin paths of the nebula and reflected into the line of sight of the observer. The contribution by free–free emission to the observed infrared flux density can be estimated using equation 7 of Roman-Lopes & Abraham (2004) and the free–free Gaunt factors of Hummer (1988). For a flux density of 884 mJy at 5 GHz (Zijlstra et al., 1990) and an electron temperature of 10000 K, the expected flux density in the K-band is about 130 Jy, which translates into $\sim 8 \times 10^{-14}$ W m^{-2} μm^{-1} at 2.2 μm. This is comparable to the continuum flux level detected across slit #1 (cf. Fig. 3). It seems, therefore, that free–fee emission does indeed dominate the continuum observed in the NIR and hides the stellar photospheres detected in the optical within the NE blob and the SW arc.

Table 3. NIR line fluxes extracted across slit #1 (between $-7\farcs5$ and $0''$) and slit #2 (between $-2''$ and $2''$).

		Line fluxes (10^{-18} W m^{-2}) $^{(a)}$	
λ (μm)	Identification	Slit #1	Slit #2
2.033	H_2 1-0 S(2)	28.3 ± 3.2	3.2 ± 1.0
2.042	He 6^3P-4^3S	7.7 ± 1.5	2.3 ± 0.5
2.058	He 2^1P-2^1S	1406 ± 39	341 ± 10
2.073	H_2 2-1 S(3)	15.0 ± 2.4	< 3
2.112	He $4^{3,1}S$-$3^{3,1}P$	84.7 ± 4.0	20.9 ± 1.2
2.121	H_2 1-0 S(1)	147.1 ± 3.5	20.5 ± 0.9
2.145	[Fe III] $^3G_3$-$^3H_4$	15.2 ± 1.4	3.5 ± 0.6
2.154	H_2 2-1 S(2)	<7	< 2
2.161	He $7^{3,1}F$-$4^{3,1}D$	61.1 ± 3.3	16.0 ± 1.1
2.165	Brγ	1994 ± 106	495 ± 27
2.198	UIR 1 $^{(b)}$	13.1 ± 2.5	2.6 ± 0.5
2.218	[Fe III] $^3G_5$-$^3H_6$	63.4 ± 1.7	15.7 ± 0.8
2.223	H_2 1-0 S(0)	45.6 ± 2.2	7.1 ± 1.0
2.242	[Fe III] $^3G_4$-$^3H_4$	25.5 ± 1.3	7.6 ± 1.3
2.247	H_2 2-1 S(1)	14.3 ± 1.1	< 5
2.286	H_2 3-2 S(2)	15.8 ± 1.8	4.0 ± 1.0
2.340	H I 31–5	11.4 ± 3.4	3.9 ± 1.2
2.344	H I 30–5	16.0 ± 4.8	< 8
2.349	H I 29–5 $^{(c)}$	60.7 ± 18.2	12.5 ± 3.7
2.354	H I 28–5	16.4 ± 4.9	3.1 ± 0.9
2.360	H I 27–5	20.1 ± 6.0	3.8 ± 1.1
2.367	H I 26–5	28.0 ± 8.4	5.1 ± 1.5
2.374	H I 25–5	19.7 ± 5.9	5.0 ± 1.5
2.383	H I 24–5 $^{(d)}$	51.4 ± 15.4	10.4 ± 3.1

$^{(a)}$ Errors are at the 1σ level and only include the uncertainties coming from the fitting procedure. In the case of the H I Pfund series, we give a larger error of the order of 30% because of the uncertainty fitting the continuum. $^{(b)}$ The H_2 3-2 S(3) transition at 2.201 μm is observed in regions 1 and 4 of slit #1 (see Table 4). $^{(c)}$ This line is probably blended with a transition of [Fe III]. $^{(d)}$ This line is likely contaminated by atmospheric lines.

Moving along slit #1 and from NE to SW, we only start detecting emission from Brγ at the ($0''$,$0''$) position, i.e. the location of the continuum within the NE blob. After this position, the Brγ line flux slowly increases, reaching a local maximum $1\farcs25$ ahead of the NE blob and coincident with the weaker blob detected in the acquisition image. It then reaches a minimum within the nebula and increases rapidly afterwards. This bright portion corresponds to the SW arc structure seen in the image and reaches an absolute maximum $5\farcs5$ ahead of the NE blob.

Moving along slit #2, the Brγ emission resembles that of a shell structure, with two maxima at the edge of the ionized

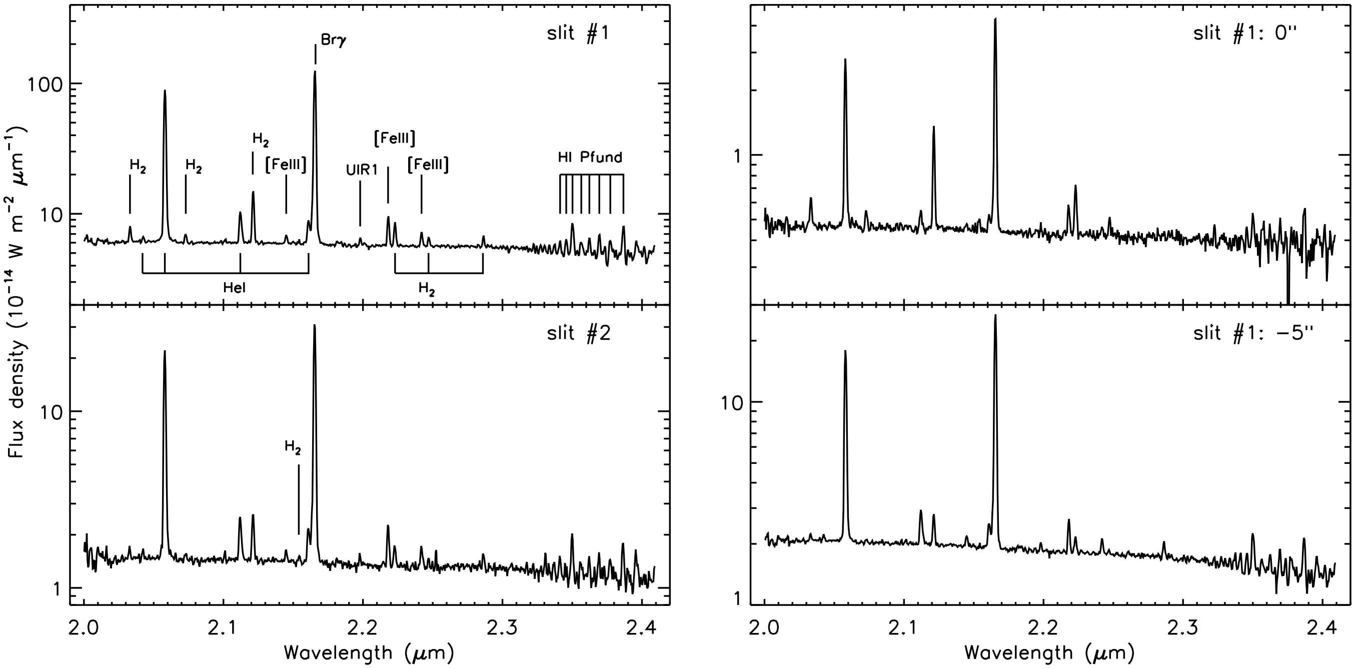

Fig. 3. **(Left)** Spectra of M1–78 extracted across (top) slit #1 between –7″.5 and 0″ and (bottom) slit #2 between –2″ and 2″(see Fig. 1). The observed lines, their identification and their line fluxes are listed in Table 3. **(Right)** Spectra extracted across slit #1 from 0″.75×0″.75 regions around the continua detected within the NE blob (top) and the SW arc (bottom). Note the logarithmic scale of the flux axis.

nebula (at about –1″ and 2″.5) and a decreased emission within the nebula.

The following panels compare the He I distributions of the 2.058 and 2.112 μm lines to that of the Brγ. It is noticeable that while the 2.112 μm He I line spatial variation traces the Brγ emission well, this is not the case of the 2.058 μm He I line. This difference will be discussed in detail in Sect. 4.4.

The spatial variation in the H_2 1-0 S(1) transition at 2.121 μm is also plotted in Fig. 4. The H_2 emission extends over ~30″ across slit #1 and ~20″across slit #2. We distinguised four different regions in slit #1 and three in slit #2, which will be analysed separately in Sect. 4.7.

M1–78 has also been observed using the mid-infrared long-slit spectrograph SpectroCam-10 mounted on the 5 m Hale Telescope at Palomar Observatory (cf. Peeters, 2002). These observations were taken using a slit of 1″×16″.4 slit positioned along the same axis of our slit #1 and centered on the brightest spot. Figure 5 compares the spatial variations of the [Ne II] line at 12.8 μm and the flux at 12 μm with the Brγ profile. Both silicate in emission and dust continuum contribute to the flux at 12 μm. The variation of the [Ne II] line traces that of Brγ well, with only a small variation close to the NE blob. The "dust" profile shows a cavity within the nebula and a clear shell-like structure, suggesting that the dust have been removed from within the ionized gas volume either through radiation pressure from the star within the NE blob or destruction. In contrast, in the arc, the "dust" emission concides with that of the ionized gas.

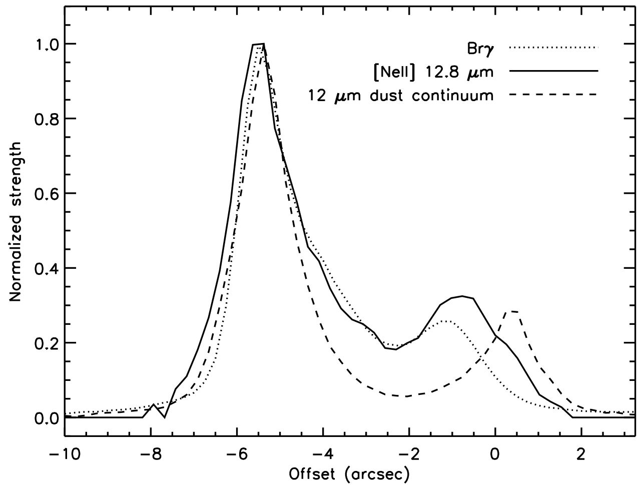

Fig. 5. Spatial variation of the [Ne II] 12.8 μm fine-structure line (solid line) and the 12 μm dust continuum (dashed line) obtained with the mid-infrared spectrograph SpectroCam-10 mounted on the 5 m Hale Telescope at Palomar Observatory. These variations correspond to a 1″×16″.4 slit positioned along the same axis of our slit #1. We show the Brγ variation (dotted line) for comparison.

4.3. Unidentified features

Several unidentified features are also present. Two relatively common unidentified features at 2.1981 and 2.2860 μm are present in the *K*-band spectra of e.g. Orion (cf. Luhman et al., 1998) and PNe (cf. Luhman & Rieke, 1996; Hora & Latter,

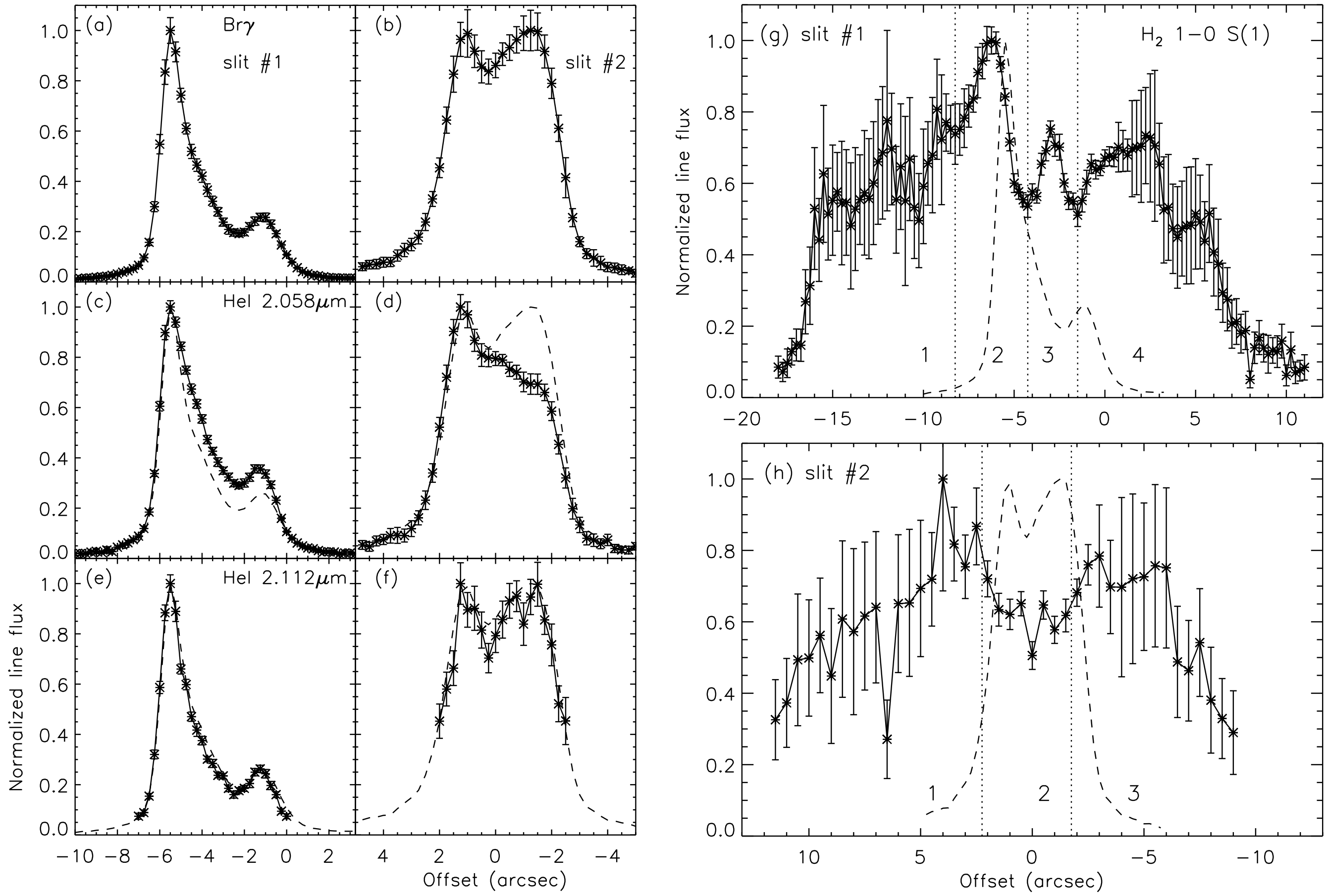

Fig. 4. (Left) Spatial variation of Brγ and the two strongest He i lines at 2.058 and 2.112 μm across slit #1 (left) and slit #2 (right). The normalized He i intensity distributions are compared to the Brγ profile (dashed line). **(Right)** Spatial variation of the H_2 1-0 S(1) transition at 2.121 μm across slit #1 (top) and slit #2 (bottom) compared to the Brγ profile (dashed line). The different regions analysed in the text are identified (dotted lines). The origin corresponds to the (0″,0″) position of Fig. 1.

1996; Hora et al., 1999; Lumsden et al., 2001b), quite close to the 3–2 S(3) and 3–2 S(2) transitions of H_2 at 2.2008 and 2.2864 μm, respectively, where these are the air wavelengths. This is discussed at length by Geballe et al. (1991), who examined lists of permitted and forbidden atomic lines for wavelength coincidences with these features and only found near coincidences with weak lines. Geballe et al. claimed that the parent ion responsible for these features corresponds to an excitation level between 30 and 60 eV, but the higher end of this range is inconsistent with the observed presence of these lines in objects with effective temperatures $<$ 40000 K (cf. Lumsden et al., 2001b). Dinerstein (2001) claimed an identification for these features as [Kr iii] and [Se iv] for the 2.198 and 2.286 μm lines, respectively. However, the abundance of both krypton and selenium in the interstellar medium is sufficiently low that this remains a mystery.

In the integrated spectra shown in Fig. 3, we detect two lines at 2.1981 ± 0.0001 μm and 2.2864 ± 0.0001 μm. While the former line is coincident with the unidentified feature discussed by Geballe et al. (and designated UIR 1), the other line can be unquestionably identified as the 3–2 S(2) transition of H_2. We however note that the 3–2 S(3) transition of H_2 (with an observed central wavelength at 2.2008 ± 0.0001 μm) is detected in regions 1 and 4 of slit #1, well outside the ionized gas region (cf. Fig. 4). In these two regions, the UIR 1 feature is not detected. The UIR 1 feature is not detected either in regions 1 and 3 of slit #2. This behavior suggests that the carrier of this unidentified UIR 1 line is probably an ion created by UV photons of at least 13.6 eV.

4.4. Analysis of the He i recombination lines

Calculations of the He i recombination cascade spectrum have been published by different authors, e.g. Smits (1991, 1996) and Benjamin et al. (1999, 2002). Each study improved the prior treatment of physical processes, mainly as the result of improved theoretical calculations of various rates. The He i recombination cascade spectrum has been recently revisited by Bauman et al. (2005) and Porter et al. (2005, 2007) using improved radiative and collisional data. They use highly accurate calculations of the *J*-resolved transition probabilities that take singlet–triplet mixing into account. Calculations of collisionless (low-density limit) Case B He i emissivities are published by Bauman et al. (2005). The source of the *J*-resolved code used in these calculations is available online (see Porter, 2007).

Theoretical predictions of several He I line ratios are shown in Fig. 6. We used the calculations of Porter (2007), which are only available for the low density limit and for $\tau_{3889} = 0$, and those of Benjamin et al. (1999), whose predictions consider different values of n_e and τ_{3889}. Here, τ_{3889} is the line center optical depth of the 3^3P–2^3S 3890 Å line. Since the ratios are rather insensitive to n_e, we only represented the curves of Benjamin et al. (1999) for $n_e = 10^4$ cm^{-3} but varying T_e from 5000 to 12500 K and τ_{3889} from 0 to 100. From the figure, it can be seen that the theoretical predictions of Porter (2007) with T_e between 8000 K and 10000 K reproduce the data well, whereas the calculations of Benjamin et al. (1999) give temperatures somewhat lower than 8000 K for $\tau_{3889} = 10$. These values of T_e – corresponding to that characteristic of the He$^+$ zone of the nebula – are lower than those obtained from the [N II] line ratios. This is a rather common behavior in Galactic HII regions, as can be found in the Orion Nebula (Esteban et al., 2004), NGC 3576 (García-Rojas et al., 2004) and others. The difference between T_e obtained from collisionally excited and recombination lines could be related to the presence of temperature fluctuations in ionized nebulae (e.g. Peimbert, 1967).

Figure 4 shows that while the He I 2.112/Brγ ratio is fairly constant across the slits, there nevertheless exists a large spatial variation in the He I 2.058μm line with respect to Brγ and the other He I recombination lines. For instance, the He I 2.058/2.112 ratio varies between 10 and 25, reaching its lowest values at positions $< -5''$for slit #1 and $> 0''$for slit #2. The origin of this spatial variation is not clear. To first order, temperature variations should have similar effects on all the lines, so this is probably not the cause. Density variations, on the other hand, might be able to produce the observed effect but would in principle not be measureable. The most probably cause of this effect seems to be optical depth variations across the nebula.

The theoretical calculations of Bauman et al. (2005) fail to reproduce the He I 2.058μm line. For instance, they predict a He I 2.058/2.112 ratio around 0.3–0.4. Evidently, the line flux of the He I 2.058μm line is largely underpredicted. The models of Benjamin et al. (1999), on the other hand, predict a He I 2.058/2.112 ratio between 20 and 50 for large variations of τ_{3889}, density and temperature. Hence, models seem incapable of fitting the He I 2.058μm line. This is because this line is not well defined in the Case B approximation: e.g. the Bauman et al. code assumes that the 2^1P to 1^1S photons are absorbed by some other atom or ion. The He I 2.058μm transition is determined by the population in the 2^1P state. The Case B approximation assumes that 2^1P to 1^1S photons do not escape the cloud, but does that mean that they are reabsorbed and completely converted to 2^1P to 2^1S photons, or that they are destroyed or absorbed by some other atom or ion? This effect, negligible for every other line, has an enormous effect on the 2.058 μm line.

4.5. The H I Pfund lines

The forest of lines redward of about 2.3 μm corresponds to the higher members of the atomic H I Pfund series. We detected H I pfund series lines from Pf24 to Pf31 which allowed us to infer the extinction across the K-window when compared with the theoretical predictions of Hummer & Storey (1987) and Storey & Hummer (1995). These lines are consistent with an extinction $A_K < 1$ in agreement with the optical estimate.

4.6. Forbidden iron lines

We report the detection of [Fe III] emission. The K-band hosts [Fe III] lines from the multiplet connecting the ^{3}G and ^{3}H terms (e.g. figure 6 of Bautista & Pradhan, 1998). Of the four transitions in this multiplet with relatively large (magnetic dipole) transition probabilities, three are in this wavelength region: 2.145, 2.218 and 2.242 μm. The fluxes measured for these lines are listed in Table 3. Since these lines originate from highly excited levels, their absolute emissivities are quite sensitive to the temperature. However, the line ratios are primarily sensitive to the density.

We compared our observed [Fe III] line ratios with theoretical predictions. We used the calculations of Keenan et al. (2001) and the more complete ones provided by M. Rodríguez (Rodríguez, 2002). These last calculations use a 33-level model atom where all collision strengths are those calculated by Zhang & Pradhan (1997), the transition probabilities those recommended by Froese Fischer & Rubin (1998) (and those from Garstang, 1958, for the transitions not considered by Froese Fischer & Rubin), and the level energies have been taken from the NIST database. We considered densities between 10^2 and 10^5 cm^{-3}. In Fig. 7 we can see that our data points are consistent with the predictions of Rodríguez, giving densities on the order of those determined from the optical forbidden lines. However, the predictions of Keenan et al. fail to fit the observed 2.242/2.218 μm ratios; this is also the case for the theoretical predictions of Bautista & Pradhan (1998), who overpredict the observed 2.242/2.218 μm ratios by factors between ~1.5 and 2.5.

4.7. H_2 excitation

The NIR emission from H_2 can be produced by either thermal emission in shock fronts or fluorescence excitation by non-ionizing UV photons in the Lyman–Werner band (912–1108 Å). These mechanisms can be distinguished since they preferentially populate different levels producing different spectra. For shock-excited H_2 the lower energy levels are typically populated as for a gas in local thermal equilibrium (LTE) with a characterisitic excitation temperature around 1000 K. In contrast, for radiatively excited gas the population follow a non-LTE distribution characterized by high excitation temperatures around 10 000 K and lines from high vibrational levels ($v \gg 1$) may be detected.

Non-thermal excitation mechanisms readily excite the $v = 2$ and higher vibrational states, whereby collisional transitions preferentially de-excite the $v = 2$ level in favor of the $v = 1$ level. Hence, the H_2 1–0 S(1)/2–1 S(1) ratio has on occasion been used to distinguish between these two processes. However, in dense clouds, FUV irradiation can

Table 4. Air wavelengths, upper energy levels, Eistein A coefficients, degeneracies and line fluxes of the H_2 lines detected in M1–78. We also give significant line flux ratios and results such as the ortho-to-para ratio (ϕ) and the excitation temperature.

Transition	λ_j	E_j	A_j	g_j	Slit 1 (a)				Slit 2 (a)		
	(μm)	(K)	(10^{-7} s)		Region 1	Region 2	Region 3	Region 4	Region 1	Region 2	Region 3
1-0 S(2)	2.0332	7584	3.98	9	35.3 ± 2.6	18.5 ± 1.9	10.4 ± 1.1	26.3 ± 1.1	8.0 ± 1.4	2.9 ± 0.7	5.3 ± 1.0
2-1 S(3)	2.0729	13890	5.77	33	16.7 ± 1.9	9.9 ± 1.1	4.6 ± 0.6	22.3 ± 1.1	5.9 ± 1.1	< 3	3.1 ± 0.7
1-0 S(1)	2.1212	6956	3.47	21	148.6 ± 10.4	92.3 ± 1.4	48.5 ± 1.2	150.8 ± 3.6	44.5 ± 2.3	19.1 ± 0.8	30.1 ± 1.9
2-1 S(2)	2.1536	13152	5.60	9	< 3.5	< 4.2	< 2.5	10.7 ± 1.1	3.6 ± 0.9	< 2	< 3
3-2 S(3)	2.2008	19086	5.63	33	5.7 ± 1.4	< 4.2	< 2.2	8.5 ± 2.3	< 3	< 3	< 2
1-0 S(0)	2.2229	6471	2.53	5	33.8 ± 3.8	28.5 ± 2.2	16.6 ± 0.8	38.3 ± 1.7	11.6 ± 1.5	6.9 ± 1.0	< 5
2-1 S(1)	2.2471	12550	4.98	21	15.1 ± 2.2	9.3 ± 1.1	4.2 ± 0.7	16.3 ± 1.6	5.0 ± 1.1	< 4	4.0 ± 1.1
3-2 S(2)	2.2864	18386	5.63	9	< 3.3	11.6 ± 1.3	4.0 ± 0.6	< 4.5	< 3	4.4 ± 1.0	2.3 ± 1.0
1-0 S(1)/2-1 S(1)					9.8 ± 1.6	9.9 ± 1.2	11.5 ± 1.9	9.2 ± 0.9	8.6 ± 1.9	> 4	7.5 ± 2.1
1-0 S(1)/3-2 S(3)					26.1 ± 6.6	> 22	> 22	17.6 ± 4.8	> 17	> 7	> 15
ϕ_1					3.5 ± 0.3	3.1 ± 0.2	2.9 ± 0.2	3.7 ± 0.1	3.6 ± 0.4	3.3 ± 0.4	(b)
ϕ_2					△	△	△	2.0 ± 0.2	1.7 ± 0.4	(c)	(c)
T_{ex} (K) (e)					980 ± 165	720 ± 55	690 ± 20	720 ± 150	750 ± 175	570 ± 55	590 ± 120
T_{ex} (K) (f)					2255 ± 230	2100 ± 260	1910 ± 330	2465 ± 390	2380 ± 330	(d)	2265 ± 420

(a) Line fluxes are given in units of 10^{-18} W m^{-2}. (b) The 1-0 S(0) line was not been measured. (c) Only one or two $v = 2$ lines were detected. (d) There are only upper limits for the $v = 2$ transitions. (e) Excitation temperature determined from the $v = 1$ states only. (f) Excitation temperature determined from the $v = 1$ and $v = 2$ states.

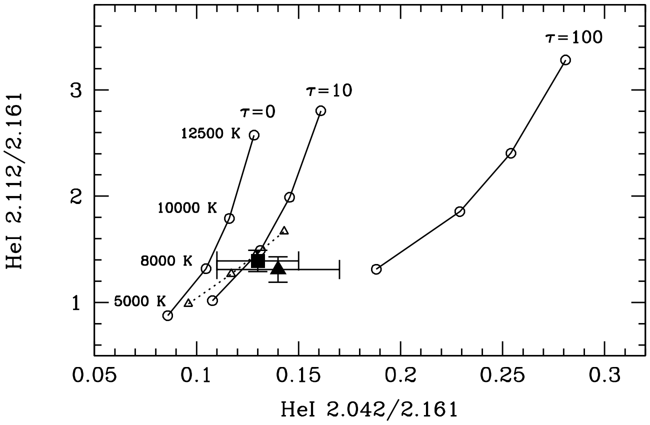

Fig. 6. Plot of the He I 2.112 $4^{3,1}$S–$3^{3,1}$P/2.161 $7^{3,1}$F–$4^{3,1}$D ratio against the He I 2.042 6^3P–4^3S/2.112 $4^{3,1}$S–$3^{3,1}$P ratio. Ratios measured for slit #1 are plotted by a black square, and by a black triangle for slit #2. The open triangles represent the theoretical predictions using the J-resolved code of Bauman et al. (2005) for T_e = 5000 K, 8000 K, 10000 K and 12500 K. Similarly, the open circles represent the predictions of Benjamin et al. (1999) for the same electron temperatures and three values of τ_{3889}: 0, 10 and 100.

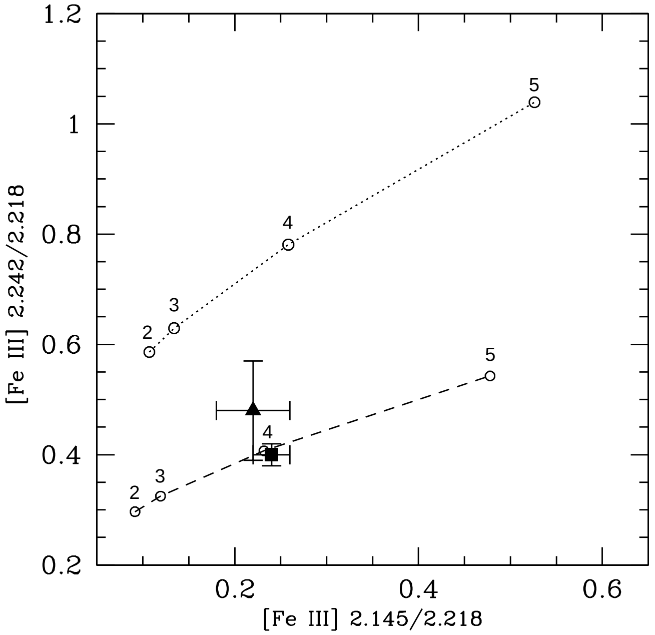

Fig. 7. K-band [Fe III] line ratios. We show the theoretical predictions of Keenan et al. (2001) (dotted line) and Rodríguez (2002) (dashed line) for densities between $\log n_e$ = 2 and $\log n_e$ = 5. The black square and triangle represent the line ratios measured for slit #1 and slit #2, respectively.

heat the gas to temperatures ~1000 K leading to collisionally excited and thermalized 1–0 line emission, while direct FUV pumping maintains non-thermal fluorescent populations in higher-lying vibrational levels (e.g. Sternberg & Dalgarno, 1989; Draine & Bertoldi, 1996). Hence, for low densities ($n_H \sim 10^3$ cm^{-3}), the 1–0 S(1)/2–1 S(1) ratio retains a pure fluorescence value around 2. But for high density clouds ($n_H \gtrsim 10^3 - 10^4$ cm^{-3}) and an intense incident FUV radiation field with $G_0 \gtrsim 10^4$ (where G_0 is the incident FUV photon flux between

6 and 13.6 eV measured in units of the local interstellar radiation field), the 1–0 S(1)/2–1 S(1) ratio will rapidily approach a thermal value of about 10 (e.g. Hollenbach & Natta, 1995), which has often been interpreted to indicate shock emission. Conversely, the 1–0 S(1)/3–2 S(3) ratio retains a value of approximately 8 in a dense photodissociation region (PDR) when $G_0 \sim 10^3$ and only for very high densities and a very intense FUV radiation field ($n_\mathrm{H} \gtrsim 10^5$ cm^{-3} and $G_0 \gtrsim 10^4$) will this ratio approach a thermal value of 10–100 (Hollenbach & Natta, 1995). Therefore, the combination of the 1–0 S(1)/2–1 S(1) and 1–0 S(1)/3–2 S(3) ratios should in principle serve as an indicator of the excitation mechanism of the H_2.

We distinguished four different regions along slit #1 and three along slit #2 with sufficient signal-to-noise (cf. Fig. 4). The line fluxes measured for all these regions are listed in Table 4. This table also lists the values for the 1–0 S(1)/2–1 S(1) and 1–0 S(1)/3–2 S(3) ratios. Across slit #1, the 1–0 S(1)/2–1 S(1) remains practically constant within the errors with an average value around 9.7 ± 0.6. The 1–0 S(1)/3–2 S(3) ratio is in general higher than 20 for all these regions. A similar scenario occurs for the three regions along slit #2. Both ratios suggest thermal emission. However, in the case of a dense PDR with $n_\mathrm{H} \gtrsim 10^5$ cm^{-3} and a very intense FUV radiation field with $G_0 \gtrsim 10^4$, these ratios can be explained by a non-thermal excitation mechanism. We can now estimate if the PDR in M1–78 can effectively be characterized by such high values of G_0 and n_H.

G_0 can be derived by assuming that all the UV photons are absorbed in a spherical shell of the size of the PDR and re-emitted in the infrared continuum (cf. Bernard-Salas & Tielens, 2005). Normalizing G_0 to the average interstellar field (1.6×10^{-6} W m^{-2}; Habing, 1968), the expression is:

$$G_0 = \frac{4F_\mathrm{IR}}{1.6 \times 10^{-6} \times 2.35 \times 10^{-11} \theta^2} , \tag{1}$$

where θ is the diameter of the PDR in arcseconds and F_IR is the observed infrared flux in W m^{-2}. We use a FIR flux of $\sim 7 \times 10^{-12}$ W m^{-2} determined by fitting a blackbody through the IRAS fluxes at 25, 60 and 100 μm (Peeters et al., 2002). We obtain a G_0 around $(1-2) \times 10^3$ considering a size of 20″–30″ (see Fig. 4). We note, however, that G_0 might be substantially larger if the filling factor of the PDR gas is small.

The total density can be determined, for instance, using fine-structure lines emitted in the PDR. The O I 63μm/[C II]158μm ratio is a good tracer for densities in between 10^3 and 10^6 cm^{-3} because these two lines have different critical densities. These two lines have been measured by ISO within an aperture of ∼ 80″ (Peeters et al., 2002). With a ratio of 7.5 ± 0.6, the models by Kaufman et al. (1999) indicate a density of $10^4 - 10^5$ cm^{-3} when $G_0 \gtrsim 10^3$.

Therefore, it seems reasonable to assume the case of a very dense PDR and a strong radiation field. This analysis, however, is not conclusive and we will use two additional diagnostics to clarify the origin of the H_2 emission: the ortho-to-para ratio and the excitation diagrams.

4.7.1. The ortho-to-para ratio

An additional diagnostic is provided by the ortho-to-para ratio. At the moment of formation, molecular hydrogen can join one of two denominations: ortho (aligned nuclear spins) or para (opposed nuclear spins). The ortho-to-para ratio ϕ, based on the statistical weights of the nuclear spins, is 3:1. In outflow regions where shock excitation is the primary emission mechanism, observations of vibrational emission lines typically reveal ortho-to-para ratios for vibrationally excited states that are comparable to 3 (e.g. Smith et al., 1997), as is expected if the gas behind such shocks is in LTE. However, as discussed at length by Sternberg & Neufeld (1999), the ortho-to-para ratio can take values other than the intrinsic 3 if the excitation is caused by UV fluorescence, since the transitions are pumped by optically thick UV transitions in which the optical depth depends on whether the molecule is in an ortho or para state. Indeed, ratios in the range 1.5–2.2 have been measured in PDRs (e.g. Ramsay et al., 1993; Chrysostomou et al., 1993; Shupe et al., 1998; Lumsden et al., 2001a).

From the 1–0 S(0), 1–0 S(1) and 1–0 S(2) line fluxes, we measured the ortho-to-para ratio for the $v = 1$ states (ϕ_1) following equation 9 of Smith et al. (1997). In Table 4 we list the $v = 1$ ortho-to-para ratio for each region. These are consistent with a ratio of 3 suggesting a thermalization of the $v = 1$ states. Of course, they do not tell the whole story. In a few cases, a value of the ortho-to-para ratio for the $v = 2$ states (ϕ_2) was derived from the 2–1 S(1), 2–1 S(2) and 2–1 S(3) transitions using equation 1 of Davis et al. (2003). We obtained ratios around 2, typical of PDRs and in agreement with the ratios derived by Lumsden et al. (2001b).

4.7.2. H_2 excitation diagrams

The simplest way of characterizing the molecular hydrogen emission, however, is to plot the observed column density against the energy of the upper level. The measured intensity, I, of a given H_2 line can be used to calculate the column density of the upper excitation level of the transition, which, for optically thin emission, is given by:

$$N_j = \frac{4\pi\lambda_j I}{A_j hc} , \tag{2}$$

where λ_j is the rest wavelength and A_j is the Einstein A-coefficient taken from Turner et al. (1977). If collisional de-excitation is assumed to dominate, the H_2 will be in LTE and the energy levels will be populated in a Boltzmann distribution. The relative column densities of any two excitation levels can thus be expressed in terms of an excitation temperature T_ex:

$$\frac{N_i}{N_j} = \frac{g_i}{g_j} \exp\left[\frac{-(E_i - E_j)}{kT_\mathrm{ex}}\right] , \tag{3}$$

where g_j is the degeneracy, E_j is the energy of the upper level taken from Dabrowski (1984) and k is the Boltzmann's constant. The values of λ_j, E_j, A_j and g_j for the lines detected in the spectra are shown in Table 4. Clearly, plotting the logarithm of

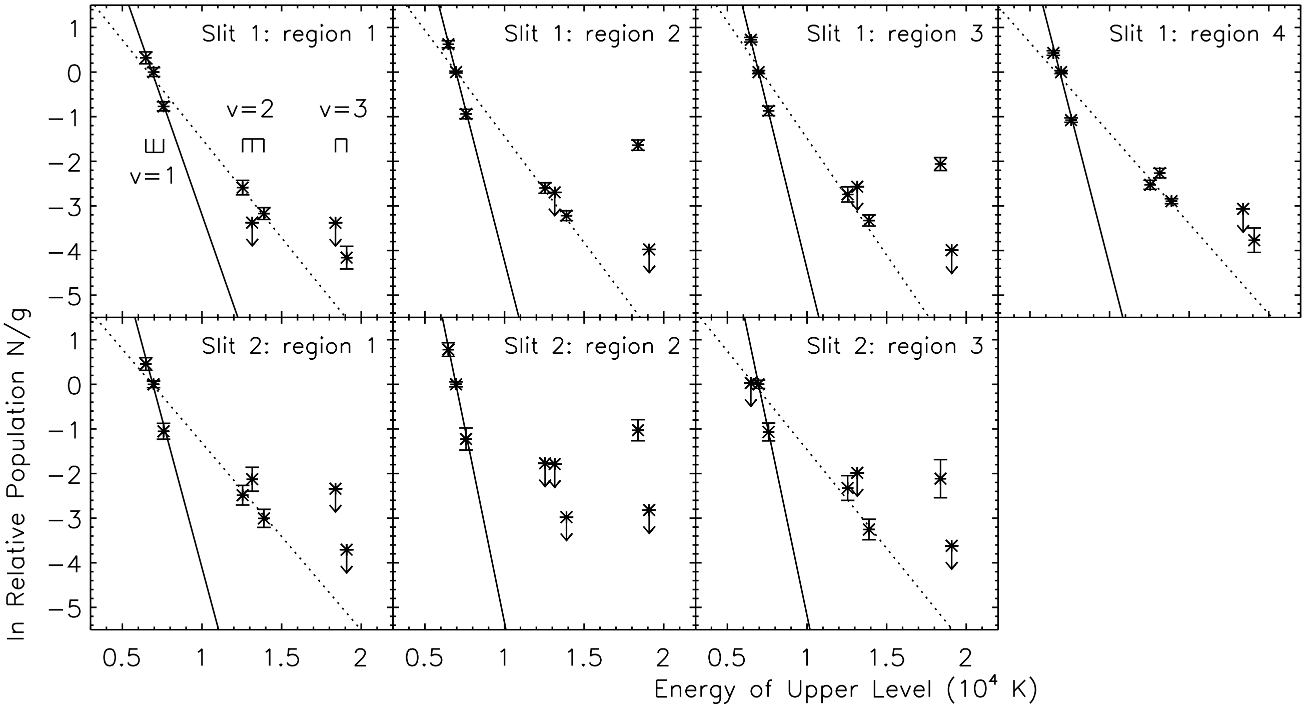

Fig. 8. H_2 excitation diagrams for each region. The lines represents the best fitting purely thermal single-temperature models. The solid line is the fit to the $v = 1$ level only and the dotted line is the fit to all the data except the $v = 3$ level.

the ratio of the column densities divided by the appropiate statistical weights gives the excitation temperature from the slope of the data.

In Fig. 8 we show plots of $\log N_j/g_j$ versus the energy for each region. We normalized the population distributions relative to that inferred from the 1–0 S(1) line. For thermalized populations at a fixed gas temperature, the $\log N/g$ points should lie on a straight line in these excitation diagrams. Cleary, such single-component models do not fit the data. While the $v = 1$ levels appear to be thermalized at $T \sim 600 - 1000$ K (solid lines), the inclusion of the $v = 2$ levels raises the best-fitting temperature to $T \sim 2000 - 2500$ K (dotted lines). Lumsden et al. (2001b) find excitation temperatures of 2400 K at the position of the nebula and slightly higher (around 3500 K) to the north and south.

However, even at these high temperatures, the $v = 3$ levels remain underpopulated and the excitation temperature inferred from the relative populations in the $v = 2$ and $v = 3$ levels exceeds 4000 K. At such gas temperatures, the molecules would be rapidly dissociated, suggesting that a non-thermal excitation mechanims is responsible for the excitation of the $v = 2$ and $v = 3$ levels.

The results of these diagrams indicate again that the observed H_2 excitation is produced in a dense PDR rather than in shocks. In fact, a high vibrational excitation temperature, such as the 4000 K inferred from the relative $v = 2$ and $v = 3$ populations, is a basic characteristic of FUV-pumped fluorescent emission (e.g. Burton et al., 1990). Furthermore, and as pointed out by Davies et al. (2003), an additional signature of fluorescent excitation appears to be present in the data. For those regions in which the 2–1 S(1), S(2) and S(3) lines are detected (region 4 in slit #1 and region 1 in slit #2), the resulting N/g values for the j=3, 4 and 5 levels do not appear to be thermalized. Instead, the $j = 4$ para-level is shifted above the adjacent $j = 3$ and $j = 5$ ortho-levels. The ortho-to-para ratio for the $v = 2$ transitions appears to be out of equilibrium and suppressed below the value of 3 obtained in LTE. This is precisely what is expected in the case of FUV pumping, where the populations of the vibrationally pumped ortho-H_2 is suppressed relative to those of the para-H_2 (Sternberg & Neufeld, 1999). Indeed, we find values as low as 2 for the $v = 2$ ortho-to-para ratio.

5. Discussion: the nature of M1–78

Zijlstra et al. (1990) and Perinotto (1991) reported that the chemical composition of M1–78 is enriched in nitrogen with respect to oxygen when compared with the typical abundance pattern of H II regions. Our optical observations, much deeper than previous ones, confirm this enrichment but also indicate that it seems to be stronger in the NE blob. The blob coincides with a very faint stellar emission that can be seen in our red optical (as discussed in Sect. 4.2, the NIR continuum is on the other hand dominated by free–free nebular emission). Therefore, it seems that a process of localized chemical enrichment is taking place to the NE of M1–78, and that the star we see at the blob is its most probable source. At the blob, the nitrogen enrichment is correlated with a defficiency in the O abundance and a – dubiou – He enrichment. This abundance pattern is typical of nebular ejecta around evolved massive stars such as WR (e.g. Esteban et al., 1992) and LBV stars (e.g.

Lamers et al., 2001). The chemical composition of these nebulae reflects the product of the CNO nucleosynthesis in the H-burning zones of the parent post-main-sequence massive star.

In order to explore the likeliness of stellar ejecta in M1–78, we derived its ionized mass from the radio flux of 884 mJy at 5 GHZ obtained by Zijlstra et al. (1990). Considering a distance of 8.9 kpc and a diameter of 8.″0, we obtain n_e(rms) ∼ 6200 cm^{-3} and M(H II) ∼ 3 $M_\odot$. The fact that the n_e(rms) coincides with the n_e obtained from the optical forbidden lines indicates that the filling factor of the gas is very close to 1. The ionized mass derived for M1–78 is on the order of those found for ejecta nebulae around WR and LBV stars, typically about a few solar masses (e.g. Esteban et al., 1992; Lamers et al., 2001). However, our nominal value of 3 $M_\odot$ should be considered as an upper limit of the mass of the ejecta.

The spatial variations of the physical conditions and chemical abundances and the presence of more than one possible ionizing source indicate that M1–78 is better described as a combination of a compact H II region + ejecta. In this sense, this combined nature can explain the negative result of Hutsemekers (1997), who doubts the classification of M1–78 as an ejecta nebula due to its very large dust mass obtained from the far-infrared emission measured by the IRAS satellite. We have to consider that the ejecta nebulae that Hutsemekers (1997) uses for his comparisons are isolated and are not related to a nearby star-forming region as M1–78 presumably is. Further indirect evidence of an ejecta nebula in M1–78 comes from the aforementioned detection of strong [Ni II] emission in its spectrum. In fact, Lucy (1995) indicates that circumstellar nebulae around LBV stars are anomalous [Ni II] emitters, as has been found in the nebula around P Cygni (Johnson et al., 1992) and two objects in the LMC (Stahl & Wolf, 1986). However, the high excitation and T_e of M1–78 do not support its identification as a LBV nebula. Typically, these objects show T_e lower than 10000 K (e.g. Lamers et al., 2001; Nota et al., 1995), and very faint or even unobservable [O III] (Nota et al., 1995). Obviously, this difficulty can be obviated if there is another hotter ionizing source in the nebula apart of the hypothetical LBV star itself. In contrast, ring nebulae around WR stars show a wide range of nebular excitations and T_e, basically depending on the spectral classification of the ionizing WR star. In fact, T_e between 12000 and 14000 K have been found in nitrogen-rich nebulae ionized by early WN and WO stars as NGC 2359, S 308 or G 2.4+1.4 (Esteban et al., 1990, 1992).

Another remarkable feature of M1–78 is the expansion velocity of the ionized gas of about 25 km s^{-1} measured by Gussie & Taylor (1989). Although this fact was considered by Gussie (1995) as an indication of the PN nature of the object, such supersonic expansion velocities are also common in WR ring nebulae (e.g. Rosado, 1986) as well as in LBV nebulae (e.g. Nota et al., 1995).

A close analogue of M1–78 is N82 (Heydari-Malayeri & Testor, 1982), a compact H II region in the Large Magellanic Cloud. This object shows nitrogen enrichment and oxygen defficiency. The ejecta seem to be produced by a WC9 star and there is one additional ionizing O star in the nebula (Moffat 1991, however, argued against this classification and suggested that the presence of a WNL or Of star in N82 is more likely). The linear size, ionized mass and n_e of N82 (0.4 pc, 7 $M_\odot$ and 5500 cm^{-3}, respectively) are very similar to those of M1–78 but the higher excitation and T_e of this Galactic object would indicate that the progenitor should be a WC or WN star of an earlier – hotter – subclass.

We investigate now the possibility that a second star, specifically an O star, might be present in M1–78, e.g. at the position of the SW arc where a second stellar continuum is detected in the optical. An estimate of the spectral type of the ionizing star in H II regions based on the He I 2.112/Brγ ratio has been proposed by Hanson et al. (2002). This method relies on a measure of the ionization fraction of helium in the H II region. For very hot stars ($T_{\rm eff} \gtrsim 40\,000$ K), helium is ionized throughout the entire nebula producing a constant relative strength of the recombination lines of helium and hydrogen. For a $T_{\rm eff}$ below this value, the helium emission compared to hydrogen quickly decreases as the H II region region becomes predominantly neutral helium. Using the predictions of Bauman et al. (2005), we determined the ratio of He I 2.112 μm to Brγ when the helium is fully ionized in an H II region. Assuming n(He)/n(H) = 0.10 and an electron temperature of 10000 K, these models predict a ratio of 0.040, in perfect agreement with the observed ratio in both slits (0.042 ± 0.002, see Table 3). Assuming for now that a single O star is responsible for the ionization of the nebula, this would imply that the ionizing star must be an early O star with $T_{\rm eff} \gtrsim 40\,000$ K. This would correspond to a spectral type earlier than O5.5 V, as inferred from the new calibration of O star parameters published by Martins et al. (2005) and based on state-of-the-art stellar models.

We do indeed find a He I 2.112/Brγ ratio of 0.043 ± 0.003 at the position of the SW arc. However, this ratio is lower at the position of the NE blob; specifically, He I 2.112/Brγ = 0.029 ± 0.005 in the 0.″75×0.″75 region around the stellar continuum within the NE blob. This implies either a low electron temperature (< 5000 K) in the NE blob (which is not the case, see Section 3.2) or the presence of a colder star that is not able to fully ionize He. It therefore appears that the WR star that we suspect to be hiding within the NE blob is not solely responsible for the ionization of the nebula.

It seems reasonable, then, to assume that a early O star is present in the SW arc of M1–78. The NIR spectrum of such a massive star will be characterized by emission of [N III] at 2.115 μm but the detection of this line at intermediate spectral resolutions is difficult since it blends with the He I line at 2.112 μm. Moreover, it is not surprising that we have not detected direct signs of its presence, since the NIR emission we detect is merely nebular. Detection of stellar features in the optical spectrum is also difficult because of the high visual extinction.

The spectral type of the ionizing stars in H II regions can be also determined from radio continuum measurements. Zijlstra et al. (1990) measured 884 mJy at 5 GHz. Assuming that the nebula is dust-free, optically thin, homogeneous and ionization-bounded, this density flux gives a minimum value for logQ_0 of 48.80 dex, where Q_0 is the rate of Lyman continuum photons required to maintain the ionization of the nebula. This value of Q_0 would correspond to a star with a spectral type earlier than O6.5 V star, in perfect agreement with the previous estimate.

6. Conclusions

There is considerable controversy surrounding the nature of M1–78, a compact object located beyond both the Local arm and the Perseus arm. It was first classified as a PN and is nowadays generally considered to be a compact H II region. To investigate the nature of M1–78 further, we obtained long-slit, intermediate-resolution, optical spectroscopy with the ISIS spectrograph at the WHT. As a complement, we obtained long-slit, intermediate-resolution, NIR spectra using LIRIS, the NIR imager/spectrographer also installed at the WHT.

M1–78 is characterized by two main morphological zones, a bright arc to the SW and a blob of emission to the NE, which correspond to two peaks in the surface brightness distribution of the optical and NIR emission lines. In addition, each peak contains a featureless, very weak and unresolved stellar continuum that was detected in the optical.

The electron densities calculated from the [S II] 6717/6731 line ratio are found to be very high and similar in both zones, 6700 and 6400 cm^{-3} for the arc and the blob. These are consistent with the densities determined from the NIR [Fe III] line ratios. The electron temperature determined from the optical nebular [N II] lines, on the other hand, is substantially different in the two zones, 10900 K in the SW arc and 13400 K in the NE blob. This last temperature is atypically high for a Galactic H II region. The temperature determined from the NIR He I lines is somewhat lower, but this difference between T_e obtained from collisionally excited and recombination lines could be related to the presence of temperature fluctuations. We find as well local differences in the extinction. The spectrum of the NE blob shows a somewhat larger reddening coefficient than the SW arc, indicating a larger amount of internal dust in this zone that produces a higher A_V of about 9 mag.

The most important result, however, is the confirmation of a nitrogen enrichment in M1–78. This enrichment is stronger at the location of the NE blob. It seems that a process of localized chemical enrichment is taking place in the NE of M1–78. This N enrichment in the blob is correlated with a defficiency in the O abundance and a – dubious – He enrichment. Such abundance pattern is typical of ejecta nebulae around evolved massive stars such as WR stars and LBV stars. The high excitation and electron temperature found in M1–78 suggest that it is more likely to be a WR star: ring nebulae around WR stars show a wide range of nebular excitation and T_e while LBV nebulae usually show T_e lower than 10000 K and very faint or even unobservable [O III].

The spatial variations in the physical conditions and chemical abundances and the presence of more than one possible ionizing source indicates that M1–78 is better described as a combination of a compact H II region + ejecta. In fact, the He I 2112 μm/Brγ line ratio, which is commonly used to estimate the spectral type of ionizing stars in H II regions, indicates a hot ($T_{eff} \gtrsim 40000$ K) O star in the SW arc. In conlusion, M1–78 seems to be ionized by a WR + hot O star system. Further observations able to observe directly the phosphere of these stars will be necessary to confirm this result.

Finally, we detect H$_2$ emission wich extends over a large ($\sim 30''$) area around the ionized nebula. The analysis of the NIR H$_2$ lines, which includes estimates of the ortho-to-para ratios and excitation diagrams, indicates that the excitation mechanism is UV fluorescence. We do not find evidence of shocks.

Acknowledgements. We thank Mónica Rodríguez for her help with the theoretical predictions of the [Fe III] line ratios, and Ryan Porter for his input regarding the theoretical calculations of the He I recombination lines. During this work, NLMH has been supported by a Juan de la Cierva fellowship from the Spanish Ministerio de Ciencia y Tecnología (MCyT). This work has also been partially funded by the Spanish MCyT under project AYA2004-07466.

References

Acosta Pulido, J. A., Ballesteros, E., Barreto, M., et al. 2003, The Newsletter of the Isaac Newton Group of Telescopes (ING Newsl.), issue no. 7, p. 15-16., 7, 15
Aller, L. H. & Keyes, C. D. 1987, ApJS, 65, 405
Bauman, R. P., Porter, R. L., Ferland, G. J., & MacAdam, K. B. 2005, ApJ, 628, 541
Bautista, M. A., Peng, J., & Pradhan, A. K. 1996, ApJ, 460, 372
Bautista, M. A. & Pradhan, A. K. 1998, ApJ, 492, 650
Benjamin, R. A., Skillman, E. D., & Smits, D. P. 1999, ApJ, 514, 307
Benjamin, R. A., Skillman, E. D., & Smits, D. P. 2002, ApJ, 569, 288
Bernard-Salas, J. & Tielens, A. G. G. M. 2005, A&A, 431, 523
Burton, M. G., Hollenbach, D. J., & Tielens, A. G. G. M. 1990, ApJ, 365, 620
Chrysostomou, A., Brand, P. W. J. L., Burton, M. G., & Moorhouse, A. 1993, MNRAS, 265, 329
Churchwell, E., Terzian, Y., & Walmsley, M. 1976, A&A, 48, 331
Dabrowski, I. 1984, Canadian Journal of Physics, 62, 1639
Davies, R. I., Sternberg, A., Lehnert, M., & Tacconi-Garman, L. E. 2003, ApJ, 597, 907
Davis, C. J., Smith, M. D., Stern, L., Kerr, T. H., & Chiar, J. E. 2003, MNRAS, 344, 262
De Robertis, M. M., Dufour, R. J., & Hunt, R. W. 1987, Journal of the Royal Astronomical Society of Canada, 81, 195
Deharveng, L., Peña, M., Caplan, J., & Costero, R. 2000, MNRAS, 311, 329
Dinerstein, H. L. 2001, ApJ Lett., 550, L223
Draine, B. T. & Bertoldi, F. 1996, ApJ, 468, 269
Esteban, C., Peimbert, M., García-Rojas, J., et al. 2004, MNRAS, 355, 229
Esteban, C., Peimbert, M., Torres-Peimbert, S., & Escalante, V. 1998, MNRAS, 295, 401
Esteban, C., Vilchez, J. M., Manchado, A., & Edmunds, M. G. 1990, A&A, 227, 515
Esteban, C., Vilchez, J. M., Smith, L. J., & Clegg, R. E. S. 1992, A&A, 259, 629
Froese Fischer, C. & Rubin, R. H. 1998, Journal of Physics B Atomic Molecular Physics, 31, 1657

Galazutdinov, G. A., Musaev, F. A., Krełowski, J., & Walker, G. A. H. 2000, PASP, 112, 648
García-Rojas, J., Esteban, C., Peimbert, M., et al. 2004, ApJS, 153, 501
Garstang, R. H. 1958, MNRAS, 118, 572
Geballe, T. R., Burton, M. G., & Isaacman, R. 1991, MNRAS, 253, 75
Grandi, S. A. 1975, ApJ, 196, 465
Grandi, S. A. 1976, ApJ, 206, 658
Gussie, G. T. 1995, Publications of the Astronomical Society of Australia, 12, 31
Gussie, G. T. & Taylor, A. R. 1989, PASP, 101, 873
Habing, H. J. 1968, Bull. Astr. Inst. Netherlands, 19, 421
Hanson, M. M., Luhman, K. L., & Rieke, G. H. 2002, ApJS, 138, 35
Heydari-Malayeri, M. & Testor, G. 1982, A&A, 111, L11
Hollenbach, D. & Natta, A. 1995, ApJ, 455, 133
Hora, J. L. & Latter, W. B. 1996, ApJ, 461, 288
Hora, J. L., Latter, W. B., & Deutsch, L. K. 1999, ApJS, 124, 195
Hummer, D. G. 1988, ApJ, 327, 477
Hummer, D. G. & Storey, P. J. 1987, MNRAS, 224, 801
Hutsemekers, D. 1997, in Astronomical Society of the Pacific Conference Series, Vol. 120, Luminous Blue Variables: Massive Stars in Transition, ed. A. Nota & H. Lamers, 316
Johnson, D. R. H., Barlow, M. J., Drew, J. E., & Brinks, E. 1992, MNRAS, 255, 261
Kaufman, M. J., Wolfire, M. G., Hollenbach, D. J., & Luhman, M. L. 1999, ApJ, 527, 795
Keenan, F. P., Aller, L. H., Ryans, R. S. I., & Hyung, S. 2001, Proceedings of the National Academy of Science, 98, 9476
Kingdon, J. & Ferland, G. J. 1995, ApJ, 442, 714
Lamers, H. J. G. L. M., Nota, A., Panagia, N., Smith, L. J., & Langer, N. 2001, ApJ, 551, 764
Latter, W. B., Kelly, D. M., Hora, J. L., & Deutsch, L. K. 1995, ApJS, 100, 159
Liu, X.-W., Storey, P. J., Barlow, M. J., et al. 2000, MNRAS, 312, 585
Liu, Y., Liu, X.-W., Barlow, M. J., & Luo, S.-G. 2004, MNRAS, 353, 1251
Lucy, L. B. 1995, A&A, 294, 555
Luhman, K. L., Engelbracht, C. W., & Luhman, M. L. 1998, ApJ, 499, 799
Luhman, K. L. & Rieke, G. H. 1996, ApJ, 461, 298
Lumsden, S. L., Puxley, P. J., & Hoare, M. G. 2001a, MNRAS, 320, 83
Lumsden, S. L., Puxley, P. J., & Hoare, M. G. 2001b, MNRAS, 328, 419
Manchado, A., Barreto, M., Acosta-Pulido, J., et al. 2004, in Ground-based Instrumentation for Astronomy. Edited by Alan F. M. Moorwood and Iye Masanori. Proceedings of the SPIE, Volume 5492, pp. 1094-1104 (2004)., ed. A. F. M. Moorwood & M. Iye, 1094–1104
Martín-Hernández, N. L., Peeters, E., Morisset, C., et al. 2002, A&A, 381, 606
Martins, F., Schaerer, D., & Hillier, D. J. 2005, A&A, 436, 1049
Mathis, J. S. 1990, ARA&A, 28, 37
Minkowski, R. 1946, PASP, 58, 305
Moffat, A. F. J. 1991, A&A, 244, L9
Nota, A., Livio, M., Clampin, M., & Schulte-Ladbeck, R. 1995, ApJ, 448, 788
Peeters, E. 2002, Ph.D. Thesis
Peeters, E., Martín-Hernández, N. L., Damour, F., et al. 2002, A&A, 381, 571
Peimbert, M. 1967, ApJ, 150, 825
Peimbert, M., Torres-Peimbert, S., & Ruiz, M. T. 1992, Revista Mexicana de Astronomía y Astrofísica, 24, 155
Pequignot, D., Petitjean, P., & Boisson, C. 1991, A&A, 251, 680
Perinotto, M. 1991, ApJS, 76, 687
Phillips, J. P. 2004, MNRAS, 353, 589
Porter, R. L. 2007, ArXiv e-prints, 0705.1135
Porter, R. L., Bauman, R. P., Ferland, G. J., & MacAdam, K. B. 2005, ApJ Lett., 622, L73
Porter, R. L., Ferland, G. J., & MacAdam, K. B. 2007, ApJ, 657, 327
Puche, D., Zijlstra, A. A., Boettcher, C., et al. 1988, A&A, 206, 89
Ramsay, S. K., Chrysostomou, A., Geballe, T. R., Brand, P. W. J. L., & Mountain, M. 1993, MNRAS, 263, 695
Rodríguez, M. 2002, A&A, 389, 556
Roman-Lopes, A. & Abraham, Z. 2004, AJ, 127, 2817
Rosado, M. 1986, A&A, 160, 211
Shaver, P. A., McGee, R. X., Newton, L. M., Danks, A. C., & Pottasch, S. R. 1983, MNRAS, 204, 53
Shaw, R. A. & Dufour, R. J. 1995, PASP, 107, 896
Shupe, D. L., Larkin, J. E., Knop, R. A., et al. 1998, ApJ, 498, 267
Smith, M. D., Davis, C. J., & Lioure, A. 1997, A&A, 327, 1206
Smits, D. P. 1991, MNRAS, 251, 316
Smits, D. P. 1996, MNRAS, 278, 683
Stahl, O. & Wolf, B. 1986, A&A, 158, 371
Stasinska, G. 1978, A&A, 66, 257
Sternberg, A. & Dalgarno, A. 1989, ApJ, 338, 197
Sternberg, A. & Neufeld, D. A. 1999, ApJ, 516, 371
Storey, P. J. & Hummer, D. G. 1995, MNRAS, 272, 41
Terzian, Y., Higgs, L. A., MacLeod, J. M., & Doherty, L. H. 1974, AJ, 79, 1018
Turner, J., Kirby-Docken, K., & Dalgarno, A. 1977, ApJS, 35, 281
Whitford, A. E. 1958, AJ, 63, 201
Zhang, H. L. & Pradhan, A. K. 1997, A&AS, 126, 373
Zijlstra, A., Pottasch, S., & Bignell, C. 1990, A&AS, 82, 273